




Nanocomposite of PVA/PVP blend incorporated by copper oxide nanoparticles via nanosecond laser ablation for antibacterial activity enhancement

M. F. H. Abd El-Kader¹ · Mohamed T. Elabbasy^{2,3} · A. A. Adeboye^{2,4} ·
A. A. Menazea^{5,6} 

Received: 28 March 2021 / Revised: 12 November 2021 / Accepted: 16 November 2021 /
Published online: 27 November 2021

© The Author(s), under exclusive licence to Springer-Verlag GmbH Germany, part of Springer Nature 2021

Abstract

This work makes an investigation of Polyvinyl Alcohol (PVA)/Polyvinyl Pyrrolidone (PVP) composite scattered by copper oxide nanoparticles. Spectroscopic techniques have been utilized for studying the mechanism of the reaction between PVA/PVP and CuO NPs. Cell viability and antibacterial assessment are used for investigating the antibacterial activity of nanocomposite systems. XRD and FTIR-ATR approved the complexation and miscibility between PVA, PVP, and CuO NPs UV–Vis spectra approved the embedding of CuO NPs into PVA/PVP by the appearance of an additional peak at 336 nm. Optical parameters and bandgap calculation indicate that CuO NPs decrease the crystallinity of the nanocomposite system. DSC measurements were also studied to reveal the thermal stability of the prepared sample. The inhibition zone values of *E. coli* and *S. aureus* microorganisms increased by increasing the CuO NPs ratio in PVA/PVP to 18.5 ± 0.5 and 20.4 ± 6.0 . The responses of the fibroblast cell line to the synthesized nanocomposites showed the capacity of PVA/PVP/CuO NPs nanocomposite to be recommended for biomedical applications.

Keywords PVA/PVP · CuO NPs · Laser ablation · Antibacterial activity · Biomedical applications

Introduction

Polymer blending is considered the most interesting method employed in broad usages, such as; energy storage systems, fuel cells, and humidity sensors [1–3]. Due to its unique and sought-after properties, research on polymer blending has brought a significant shift in industrial practice and pharmaceuticals in recent years [4–6]. The

✉ A. A. Menazea
aanter7@gmail.com

Extended author information available on the last page of the article

presence of polymer in the form of films offers an opportunity to produce another variant of polymer with good mechanical, thermal, and inhibitory properties [7].

The importance of polyvinyl alcohol (PVA) as a polymer is highly rated because of its chemical and physical properties [8] over the years; research interest in this field has increased. PVA is semi-crystalline nature used widely in medical devices, because it possesses (among other things) adsorption, biocompatibility, and high solubility of water characteristics [9–11]. In addition, it is a nontoxic and low-cost polymer used in wound dressing, tissue engineering scaffolding, and as part of controlled drug delivery systems [12–14]. Polyvinyl Pyrrolidone (PVP) has a high polar group, low toxicity, biodegradable and amorphous nature with good film properties. It has two interactive sites N atom and C=O group. It acts as a protecting agent with other surfaces of inorganic compounds [15].

Over the past decade, metal nanoparticles were extensively studied because of their use in different usages [16–22]. Metal nanoparticles have a very important role in applied science and technology [23–30]. Numerous methods are used to prepare metal nanoparticles [31], such as laser ablation technique, method of chemical reduction, method of microorganism arc-discharge, photo-reduction, and bio-surfactant technique [32]. The attractive and innovative technique of laser ablation is currently and extensively employed to synthesize nanomaterials, which provide a clean, facile, and cost-effective method for preparation [33–36]. When an intense beam of laser hits the surface of the solid target, the nanoparticles are produced. It is a simple and non-contaminated technique [37].

Ionic metal oxides nanoparticles (NPs) such as CuO NPs are very interesting antimicrobial agents, because they have a high number of corners and edges, high surface areas, and many reactive sites [38]. It shows a variety of possible physical properties, and it can be easily combined with polymers to provide special physico-chemical properties to the composites. These nanoparticles, which have high surface areas and crystalline structures, can be used with a certain dose to have antimicrobial effects [39].

In this study, the structural, optical, and morphological characterization of PVA/PVP blend embedded by various ratios of CuO NPs by changing laser ablation time (3, 5, 10, and 15 min) were studied. The cell viability behavior and the antibacterial activity were performed for the prepared samples. This process provides an easy and low-cost method for preparing nanocomposite and uses it for biomedical application such as wound healing application.

Materials and method

Materials

PVA (M.W. \approx 130 K) and PVP (M.W. \approx 72 K) polymers brought from ACROS. Deionized water was used in the preparation of both PVA and PVP. The high pure copper plate was performed from Sigma-Aldrich.

Synthesis of PVA/PVP composite

0.7 gm of PVP and 0.7 gm of PVA have been dissolved in 70 ml of deionized water for 5 h at 50 °C to get a homogenous PVA/PVP composite.

Doping PVA/PVP with CuO NPs by laser ablation

CuONPs have been dispersed in PVA/PVP matrix by laser ablation. A pure copper plate with suitable dimensions has been placed in a beaker containing 10 ml of the produced PVA/PVP blend. Fundamental Nd:YAG laser beam having 1064 nm wavelength, 10 Hz repetition rate, and 3.6 W power was streamlined and focused on a copperplate via the convex lens to be on its surface to support the ablation and formation of CuO NPs in the PVA/PVP matrix. This detailed experiment called the one-potential laser ablation process was obtained and employed [40]. Copper oxide nanoparticles have been doped with PVA/PVP blend with various ratios by changing the ablation times (0, 3, 5, 10, and 15 min) as obtained in Table 1. The nanocomposite blends are stirred well and sonicated using dip sonicator Hielscher Up 100 H to affirm the good dispersion of CuO NPs into blend solution. The resulting PVA/PVP blends have been casted in plastic Petri dishes then dried in an oven at 40 °C for 36 Hours. The thickness of the nanocomposites was found to be about 0.22 mm.

Characterization techniques

XRD patterns of PVA/PVP composites embedded by different ratios of CuO NPs have been investigated by PANalytical X-Pert PRO by Cu target with K_{α} radiation of wavelength ($\lambda = 1.540 \text{ \AA}$) in Bragg angle (2θ) = (5–80°). FT-IR spectral data showed within the range 4000–400 cm^{-1} via Jasco spectrometer, 6100, Japan. UV–visible spectral data collected in the range of 180 to 1000 nm by a double beam spectrophotometer JASCO Corporation, V-570. Morphological features of films were obtained by FESEM type (Quanta FEG 250, USA). Differential scanning calorimetry (DSC-50, Shimadzu, Japan) has been used to conduct thermal analysis of the synthesized films, with a temperature range of ambient temperature to 375 °C with a heating rate of 10 °C/min.

Table 1 Contents of copper oxide nanoparticles embedded in PVA/PVP blend by laser ablation

Laser Ablation Time (min)	Content (g/L)
Zero	Zero
3	0.043
5	0.079
10	0.142
15	0.217

The human osteoblast cell line HFB4 has been grown in Dulbecco's modified Eagle medium (DMEM, Gibpco) at 35 °C to evaluate the cell viability of PVA/PVP/CuONPs nanocomposites. Cells seeded at a density of 5×10^3 cells/cm² have been grown on PVA/PVP/CuONPs nanocomposite in 12-well plates. The medium has been isolated after three days of incubation and MTT has been dispersed into each well, then the cell viability has been obtained using an optical analyzer as obtained in the following formula [41]:

The antimicrobial behavior of PVA/PVP blend embedded by various ratios of CuO NPs was performed against Gram-negative bacteria; *E. coli* and Gram-positive bacteria; *S. aureus*. PVA/PVP/CuO NPs were poured into Petri dishes containing Mueller-Hinton agar media and incubated at 38°C for 36 h. The antibacterial activity was calculated by measuring the diameter of the inhibition zone after incubation [42].

Results and discussion

X-ray Diffraction Analysis (XRD)

XRD scans offered a lot of valuable information about the compounds' scale, orientation, and crystal structure. XRD scans of PVA/PVP composite embedded by CuO NPs at various laser ablation times (0, 3, 5, 10, 15 min) at room temperature are presented in Fig. 1. Owing to the semi-crystalline structure of PVA supported by the hydrogen bonds, PVA has diffraction patterns at $2\theta = 19.6^\circ$ and 40.5° . There is

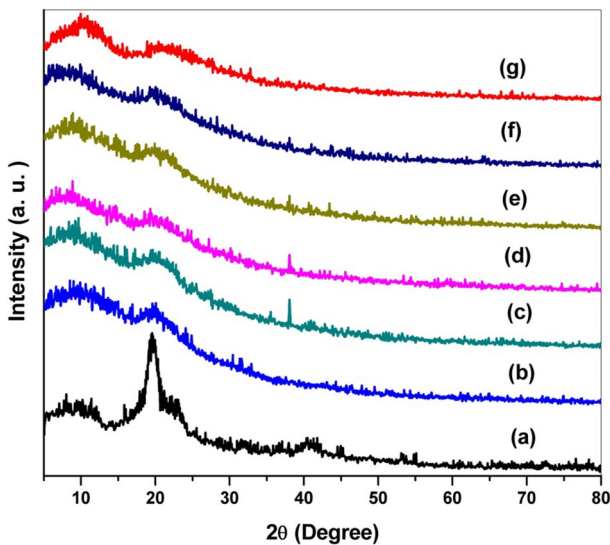


Fig. 1 XRD patterns of **a** PVA, **b** PVA/PVP, and PVA/PVP/CuO NPs at different laser ablation time **c** 3 min, **d** 5 min, **e** 10 min, **f** 15 min and **g** PVP

another diffraction pattern at $2\theta = 22.7^\circ$ with low intensity [43–45]. Hence, PVP has two semicrystalline patterns at $2\theta = 10.3^\circ$ and 21.4° [46, 47].

The PVA/PVP blend film at laser ablation time (0 min) has two diffraction patterns at $2\theta = 10.4^\circ$ and 19.6° ; this affirmed the interaction and miscibility between PVA and PVP because of the existence of O–H group in PVA and C=O group in PVP and the strong interaction between them [48].

For PVA/PVP blend films embedded by CuO NPs at various laser ablation times (3, 5, 10, 15 min), there is an additional diffraction peak at $2\theta = 38.1^\circ$ that is paralleled with CuO NPs [49]. There is a shift in the diffraction peak at $2\theta = 10.4^\circ$ towards a lower diffraction angle. As seen in Fig. 1 c–f, the intensity of peak at $2\theta = 38.1^\circ$ lowered with raising the time of ablation. This means that as more bonds were broken, new bonds were built in the polymer matrix between the blend groups and CuO NPs. Also, the peak broadening increases by raising the time of laser ablation, and this established the interaction between PVA/PVP polymer blend and CuO NPs.

The average crystal size (D) of CuO NPs is measured from XRD using Scherrer's equation;

$$D = 0.915\lambda / F \cos \theta \quad (1)$$

The crystal size of CuO NPs was 32 nm.

Fourier transform infrared (FTIR)

Figure 2 illustrates FT-IR spectra of PVA, PVP, and PVA/PVP blend films embedded by CuO NPs at various times of laser ablation (0, 3, 5, 10, 15 min). For PVA, the O–H stretching vibration has been cleared at 3305 cm^{-1} . The symmetric stretching vibrations of C–H group have been seen at 2923 cm^{-1} . The asymmetric stretching vibrations of C–H group were seen at 2852 cm^{-1} . The vibrational band at 1725 cm^{-1} was attributed to C=C stretching vibration, while O–H bending vibration was cleared at 1651 cm^{-1} . The bending vibration of C–H group was seen at 1431 cm^{-1} . The wagging vibration of C–H group was seen at 1375 cm^{-1} , respectively. At 1242 cm^{-1} , the C–H wagging of acetate residue was obtained and C–O stretching vibrations were located at 1087 cm^{-1} and 1023 cm^{-1} . At 845 cm^{-1} , the rocking vibration of CH_2 was seen [50–52]. For PVP, the stretching vibration of O–H group was obtained at 3405 cm^{-1} . The C–H bending vibrations have two bands at 1427 cm^{-1} and 1373 cm^{-1} . The C–N bending vibration was observed at 1278 cm^{-1} . CH_2 twisting and rocking vibrational bands were seen at 1220 cm^{-1} and 1012 cm^{-1} . The band at 564 cm^{-1} is assigned to N–C=O bending vibrations [53–56].

For PVA/PVP blend film at laser ablation time (0 min), there was a shift in O–H stretching vibration, in addition to the appearance of new bands at 1740 cm^{-1} , 1490 cm^{-1} , and 1250 cm^{-1} that corresponded to C=O stretching vibration, C–H bending vibration and C–O–C stretching. There was also a shift in the bands at 1644 cm^{-1} with a decrease in intensity of all bands. These results agreed with XRD analysis and confirmed the complexation between PVA and PVP [57].

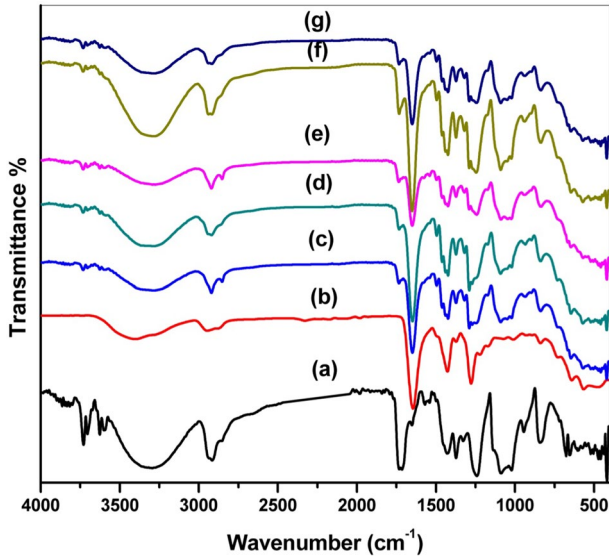


Fig. 2 FTIR-ATR of **a** PVA, **b** PVP, **c** PVA/PVP, and PVA/PVP/CuO NPs at different laser ablation time **d** 3 min, **e** 5 min, **f** 10 min and **g** 15 min

For PVA/PVP blend films embedded by CuO NPs at various times of laser ablation (3, 5, 10, 15 min), there was a slight shift in O–H stretching vibration that became broader compared to PVA/PVP polymer blend film at laser ablation time (0 min). In addition, the intensities of all bands changed irregularly with the addition of CuO NPs and ablation time. This indicates that there was an interaction between PVA/PVP and CuO NPs.

Optical properties

Figure 3 obtains UV–Vis spectra of PVA/PVP composite embedded by CuO NPs at several times of laser ablation (0, 3, 5, 10, 15 min). There was a maximum absorption peak at 225 nm in PVA/PVP composite film at laser ablation time (0 min) spectrum that corresponded to π - π^* transition of unsaturated bonds in polymer blend [58].

For PVA/PVP blend films embedded by CuO NPs at various times of laser ablation (3, 5, 10, 15 min), there was a small shift toward high wavelength. This shift correlated with the intermolecular bonding of hydrogen between the adjacent hydrogen groups in the chain of polymer and Cu ions or due to the bonding of hydrogen between C=O of PVP and Cu ions [49]. In addition, there was an additional peak at 336 nm and their intensity was raised by raising the time of laser ablation that approved the complexation between PVA/PVP and CuO NPs polymer.

It is known that Beer–Lambert law demonstrates the transfer of light through the materials according to that relation [59].

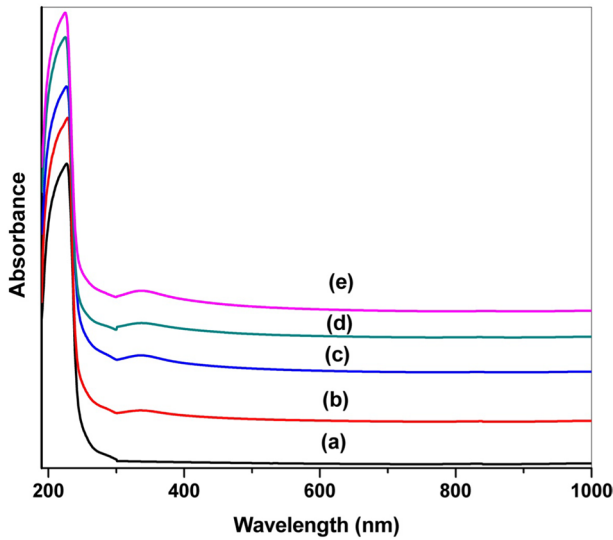


Fig. 3 UV–Vis of **a** PVA/PVP and PVA/PVP/CuO NPs at different laser ablation time **b** 3 min, **c** 5 min, **d** 10 min and **e** 15 min

$$I = I_0 e^{-\alpha d} \tag{2}$$

where I is the intensity of the transmitted light and I_0 is the intensity of the incident light, d is the thickness of the film and α is the absorption coefficient that must be analyzed in order to examine the existence of any changes in the band structure. The above relation can be written as following [60]:

$$\alpha * d = \ln \frac{I_0}{I} = \ln 10 * \log \frac{I_0}{I} = 2.303 * A \rightarrow \alpha = \frac{2.303}{d} A \tag{3}$$

where A is the absorbance.

Figure 4 obtains the relation between α and photon energy ($h\nu$). It is shown that the value of absorption edge of PVA/PVP blend was decreased irregularly by the addition of CuO NPs at various times of laser ablation (see Table 2). The shift to lower photon energy means that the bandgap lowered.

In amorphous and disordered materials, the Urbach tail has been observed and is one of the tools that is used for describing the characteristics of the electronic transition of these materials. Urbach tail width is a measure of the defect levels between the conduction and valence bands in the forbidden bandgap. Previous research showed that the absorption coefficient was represented by the Urbach relationship in the exponential-edge region [61, 62].

$$\alpha = \alpha_0 \exp \left(\frac{h\nu}{E_{ur}} \right) \tag{4}$$

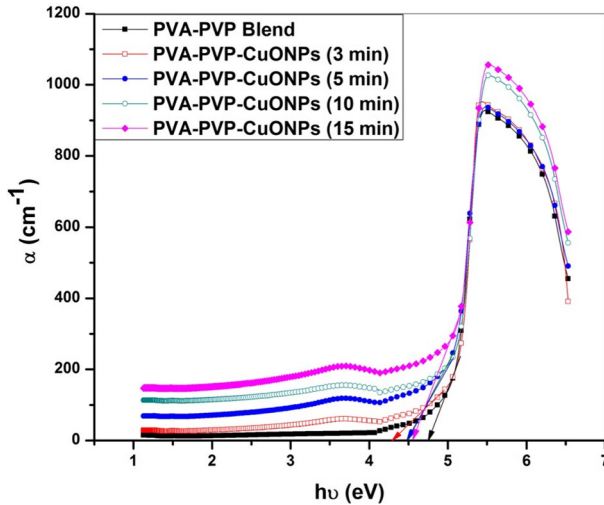


Fig. 4 Relation between α and $h\nu$ for PVA/PVP and PVA/PVP/CuO NPs at different laser ablation time (3, 5, 10 and 15 min)

Table 2 Optical parameters values of PVA/PVP blend embedded by various ratios of CuO NPs at various laser ablation time

Sample	Laser ablation time (min)	Absorption edge (eV)	Band Tail E_{ur} (eV)	Energy Gap (eV)
PVA/PVP (0 min)	0	4.74	0.17	4.40
PVA/PVP/CuO NPs (3 min)	3	4.30	0.21	3.64
PVA/PVP/CuO NPs (5 min)	5	4.49	0.24	3.36
PVA/PVP/CuO NPs (10 min)	10	4.49	0.28	2.99
PVA/PVP/CuO NPs (15 min)	15	4.55	0.36	4.29

where α_0 is a constant and E_{ur} is the width of the band tails. The relationship between $\ln\alpha$ and $h\nu$ in Fig. 5 was depicted by a straight line. Values of E_{ur} are listed in Table 2, as seen with the addition of CuO NPs and increasing the times of ablation, E_{ur} increased. The raising in E_{ur} indicates a raise in the amorphous regions in the materials. There are no sharp cutoffs for both conduction and valence bands, in amorphous materials, but in the lower energy region, they have tails of localized states.

The increase in tail width could be due to the fact that raising the CuO NPs content and ablation time in the PVA/PVP blend can contribute to the production of ionic complexes, disorders, and imperfections. This leads to a rise in localized states within the forbidden bandgap of energy [63].

Davis and Shalliday obtained the indirect and direct transitions that could be occurred near the edge of the basic band, and via plotting $(\alpha h\nu)^{1/2}$ versus $h\nu$ used to perform the optical bandgap by using this relation [64, 65].

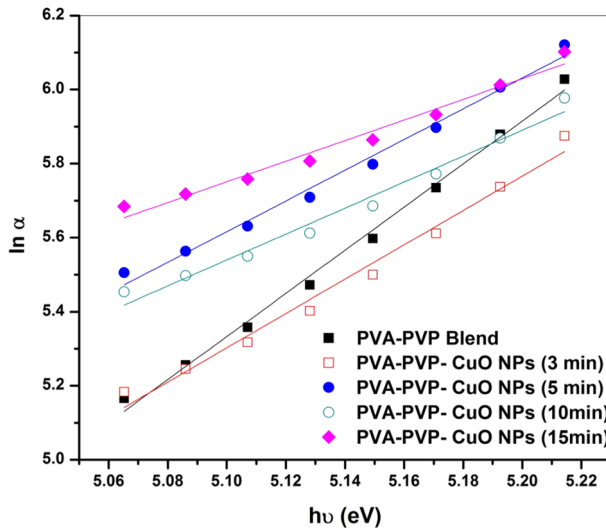


Fig. 5 Relation between $\ln \alpha$ and $h\nu$ for PVA/PVP and PVA/PVP/CuO NPs at different laser ablation time (3, 5, 10 and 15 min)

$$(\alpha h\nu)^{1/2} = B (h\nu - E_g) \tag{5}$$

The plot of $(\alpha h\nu)^{1/2}$ versus $h\nu$ is obtained in Fig. 6. As seen in Table 2 the values of indirect bandgap energy decreased compared to PVA/PVP polymer blend

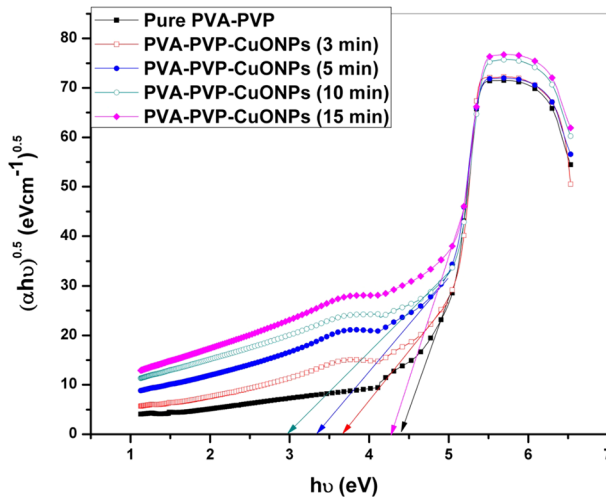


Fig. 6 Relation between $(\alpha h\nu)^{0.5}$ and $h\nu$ for PVA/PVP and PVA/PVP/CuO NPs at different laser ablation time (3, 5, 10 and 15 min)

at laser ablation time (0 min). This means that as the amorphous region in PVA/PVP blend increases, by addition of CuO NPs, the disordering increases.

Scanning Electron Microscopy (SEM)

SEM images of PVA/PVP embedded by CuO NPs are obtained in Fig. 7. SEM micrographs show the homogenous nature of pure PVA/PVP blend in Fig. 7a. Figure 7b obtains SEM photographs that show a homogenous distribution of CuO NPs through the prepared blend on its surface. CuO NPs appear on the surface as spherical white points. These white points in the high laser ablation time (15 min) were observed as big points because of the aggregations of copper oxide nanoparticles. In other words, the white points are raising as the ratio of CuO NPs raised in the PVA/PVP composite when the laser ablation time is raised. These photographs approved the distribution of CuO NPs on the surface of the PVA/PVP blend sample in semi-uniform manner.

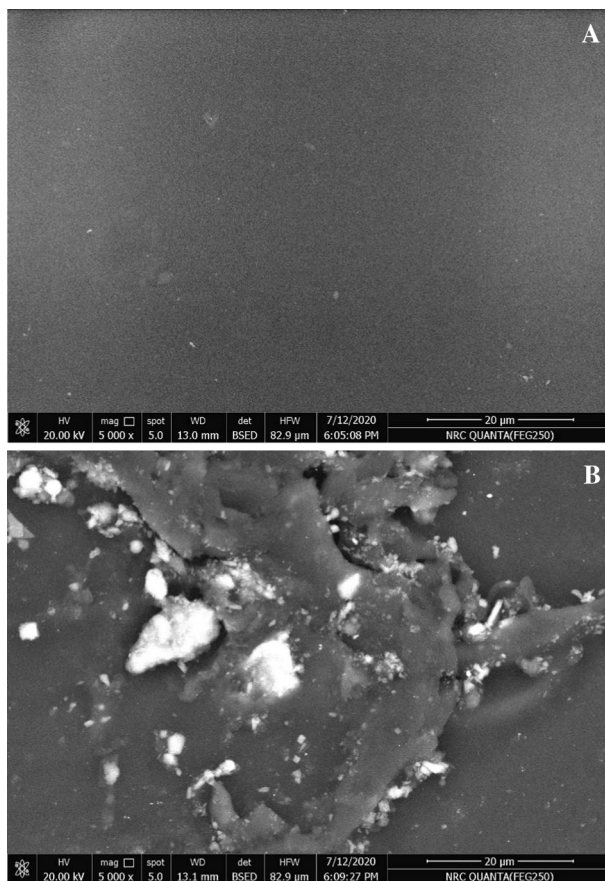


Fig. 7 FESEM photographs for PVA/PVP and PVA/PVP/CuO NPs at laser ablation time (15. min)

Differential scanning calorimetry (DSC)

Figure 8 represents the DSC thermogram of PVA, PVP, PVA/PVP and PVA/PVP incorporated with CuO NPs at various laser ablation time. As seen PVA has melting temperature at 191 °C and decomposition temperature at 316 °C [66], while PVP has melting temperature at 98 °C [67]. For PVA/PVP and PVA/PVP/CuO NPs, there is a noticeable shift to higher temperature either with blending or by additive of nano-fillers. These affirm the thermal stability of polymer nanocomposite increases with addition of CuO NPs and confirmed the intermolecular interaction between PVA/PVP polymer chains and nano-filler.

Cell viability

The responses of the cell line of fibroblasts toward PVA/PVP/CuO NPs nanocomposite predict the propensity of these films to be recommended for wound healing usages applications. The cell viability of these nanocomposites has been investigated as obtained in Fig. 9. It is evident that the cell viability of PVA/PVP matrix was $78.1 \pm 3.4\%$ and has been increased to $81.2 \pm 4.2\%$ after PVA/PVP matrix is embedded by CuO NPs via laser ablation time (3 min). The values of cell viability were increased by raising the ratios of CuO NPs inside PVA/PVP blend to $96.7 \pm 3.5\%$ for PVA/PVP blend film at laser ablation time (15 min). This is a strong indication that there is a presence of high biocompatibility of copper oxide in the PVA/PVP composite. The low ratios of CuO NPs inside PVA/PVP blend potentiate its degradation without causing fatal adverse effects. This behavior of cell viability could affect the antibacterial activity that could decrease the possible invasion and enable the development and distribution of normal cells instead of death.

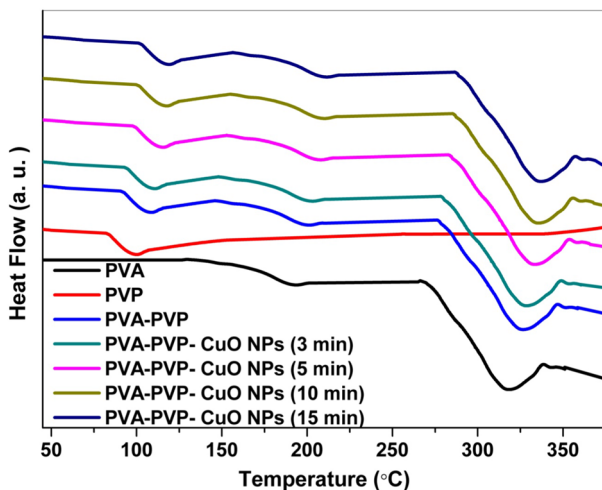


Fig. 8 DSC curves for PVA, PVP, PVA/PVP, and PVA/PVP/CuO NPs at different laser ablation time (3, 5, 10 and 15 min)

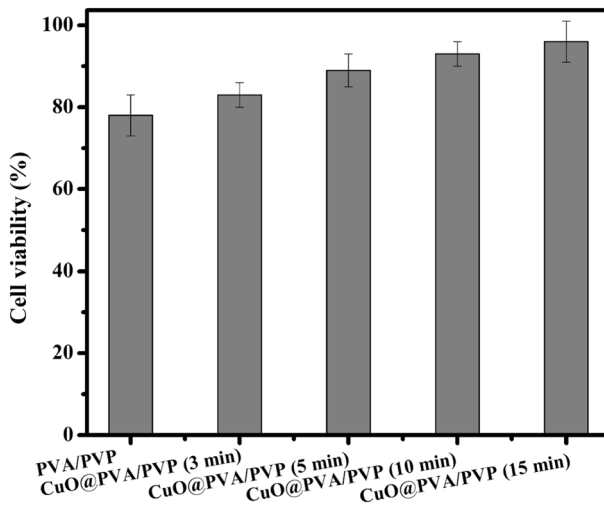


Fig. 9 Cell viability for PVA/PVP and PVA/PVP/CuO NPs at different laser ablation time (3, 5, 10 and 15 min) through HFB4 cell line in vitro

Antibacterial assessment

The potential to facilitate wound healing and other biomedical applications relies heavily on bacterial invasion inhibition, as the latter can deteriorate the cohesion of the wound. The antibacterial activity of PVA/PVP blend doped with various ratios of CuO NPs by laser ablation has been investigated against *E. coli* and *S. aureus*. As shown in Fig. 10 and Table 3, pure PVA/PVP blend (at laser time ablation (0 min)) obtain the low inhibition zone; 8.2 ± 0.5 and 9.5 ± 0.4 against *E. coli* and *S. aureus*, respectively. Moreover, the inhibition zone of PVA/PVP blend embedded in CuO NPs via laser ablation time (3 min) was 13.2 ± 0.4 and 15.4 ± 0.6 against *E. coli* and *S. aureus*, respectively. The values of inhibition zones were raised by increasing the ratios of CuO NPs inside PVA/PVP composite to 18.5 ± 0.5 and 20.4 ± 6.0 against *E. coli* and *S. aureus*, respectively, for PVA/PVP blend at laser ablation time (15 min). The antibacterial activity has been attributed to an increase in the copper oxide nanoparticles inside PVA/PVP blend and it depends on the capability of the released ionic CuO to degenerate bacterial cells [68]. The high antibacterial activity of the polymeric nanocomposite requires further investigation before it can be used in clinical applications.

Conclusion

PVA/PVP doped with different ratios of CuO NPs prepared via laser ablation (0, 3, 5, 10, 15 min) using casting technique method is characterized using XRD, FTIR-ATR, and UV-Vis techniques. Confirmation of the interaction and

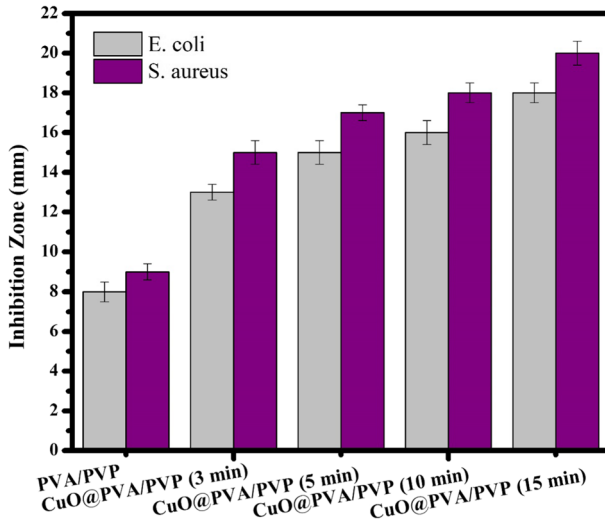


Fig. 10 Antibacterial behavior for PVA/PVP and PVA/PVP/CuO NPs at different laser ablation time (3, 5, 10 and 15 min) against *E. coli* and *S. aureus*

Table 3 Antibacterial activity of PVA/PVP blend embedded by various ratios of CuO NPs against *E. coli* and *S. aureus*

Sample code	Inhibition zone diameter (mm)	
	<i>E. coli</i>	<i>S. aureus</i>
PVA/PVP (0 min)	8.2 ± 0.5	9.5 ± 0.4
PVA/PVP/CuO NPs (3 min)	13.2 ± 0.4	15.4 ± 0.6
PVA/PVP/CuO NPs (5 min)	15.1 ± 0.6	17.3 ± 0.4
PVA/PVP/CuO NPs (10 min)	16.6 ± 0.6	18.0 ± 0.5
PVA/PVP/CuO NPs (15 min)	18.5 ± 0.5	20.4 ± 6.0

compatibility between PVA, PVP, and CuO NPs are affirmed by XRD and FTIR-ATR. UV–Vis and optical parameters showed that embedding by CuO NPs into PVA/PVP composite decreased the crystallinity of the nanocomposite system. It seems from DSC analysis that thermal stability increased by increasing CuO NPs. Antibacterial activity and cell viability have been increased with increasing CuO NPs at laser ablation time 15 min. These results could lead to the suggestion of PVA/PVP/CuO NPs for wound healing utilization.

Declarations

Conflict of interest The authors declare that they have no conflict of interest.

References

1. Gouda MH, Gouveia W, Afonso ML, Šljukić B, El Essawy NA, Nassr AA, Santos DMF (2019) Poly (vinyl alcohol)-based crosslinked ternary polymer blend doped with sulfonated graphene oxide as a sustainable composite membrane for direct borohydride fuel cells. *J Pow Sour* 432:92–101
2. Tommalieh MJ, Ibrahim HA, Awwad NS, Menazea AA (2020) Gold nanoparticles doped polyvinyl alcohol/chitosan blend via laser ablation for electrical conductivity enhancement. *J Mol Struct* 1221:128814
3. Menazea AA (2020) Pulsed laser ablation route assisted copper oxide nanoparticles doped in Polyethylene Oxide/Polyvinyl pyrrolidone blend for enhancement the electrical conductivity. *J Mol Struct* 1207:127807
4. Basha S, Rao M (2018) Spectroscopic and Electrochemical Properties of (1-x)[PVA/PVP]:x[MgCl₂H₂O] Blend Polymer Electrolyte Films. *Int J Poly Sci*, 1–11
5. Abd Elkader MF, Almogbel MS, Elabbasy MT (2020) Survival and reduction in foodborne bacteria using methyl cellulose film doped with europium oxide nanoparticles. *Food Sci Nutr* 8(1):291–298
6. Silva M, Zea Bermudez V, Pawlicka A (2020) Insight on polymer electrolytes for electrochemical devices application
7. Suganthi S, Vignesh S, Kalyanasundar JV, Raj V (2020) Fabrication of PVA polymer films with improved antibacterial activity by fine-tuning via organic acids for food packaging applications. *Appl Water Sci*, 10(4)
8. Menazea AA, Ismail AM, Awwad NS, Ibrahim HA (2020) Physical characterization and antibacterial activity of PVA/Chitosan matrix doped by selenium nanoparticles prepared via one-pot laser ablation route. *J Mate Res Tech* 9(5):9598–9606
9. Jebur Q, Hashim A, Habeeb M (2020) Fabrication, structural and optical properties for (Polyvinyl Alcohol-Polyethylene Oxide-Iron Oxide) Nanocomposites. *Egy J Chem* 63(2):611–623
10. Mostafa AM, Menazea AA (2020) Polyvinyl Alcohol/Silver nanoparticles film prepared via pulsed laser ablation: An eco-friendly nano-catalyst for 4-nitrophenol degradation. *J Mol Str*, 128125]
11. Reddy M, Chandra Babu B (2015) Structural, optical, electrical, and magnetic properties of PVA:Gd³⁺ and PVA:Ho³⁺ Polymer Films. *Ind J Mater Sci*, 1–8.
12. Ahmed MK, Mansour SF, Al-Wafi R, Menazea AA (2020) Composition and design of nanofibrous scaffolds of Mg/Se-hydroxyapatite/graphene oxide@ ε-polycaprolactone for wound healing applications. *J Mate Res Tech* 9(4):7472–7485
13. Bernal-Ballen A, Lopez-Garcia J, Merchan-Merchan M, Lehocky M (2018) Synthesis and characterization of a bioartificial polymeric system with potential antibacterial activity: Chitosan-Polyvinyl Alcohol-Ampicillin. *Mole* 23(12):3109
14. Ahmed MK, Moydeen AM, Ismail AM, El-Naggar ME, Menazea AA, El-Newehy MH (2020) Wound dressing properties of functionalized environmentally biopolymer loaded with selenium nanoparticles. *J Mol Struct* 1225:129138
15. Kaur A, Kumar R (2019) Enhanced bactericidal efficacy of polymer stabilized silver nanoparticles in conjugation with different classes of antibiotics. *RSC Adv* 9(2):1095–1105
16. Menazea AA, Abdelghany AM, Hakeem NA, Osman WH, Abd El-kader FH (2020) Nd: YAG nanosecond laser pulses for precipitation silver nanoparticles in silicate glasses: AC conductivity and dielectric studies. *Sili* 12(1):13–20
17. Feng P, Chang H, Liu X, Ye S, Shu X, Ran Q (2020) The significance of dispersion of nano-SiO₂ on early age hydration of cement pastes. *Mater Design* 186:108320
18. Zhang X, Tang Y, Zhang F, Lee CS (2016) A novel aluminum-graphite dual-ion battery. *Adv Energy Mater* 6(11):1502588
19. Zhang L, Xu Y, Liu H, Li Y, You S, Zhao J, Zhang J (2021) Effects of coexisting Na⁺, Mg²⁺ and Fe³⁺ on nitrogen and phosphorus removal and sludge properties using A2O process. *J Water Process Eng* 44:102368
20. Mostafa AM, Mwafy EA (2020) Synthesis of ZnO and Au@ ZnO core/shell nano-catalysts by pulsed laser ablation in different liquid media. *J Mate Res Tech*.
21. Chen CX, Yang SS, Ding J, Wang GY, Zhong L, Zhao SY, Ren NQ (2021) Non-covalent self-assembly synthesis of AQ2S@ rGO nanocomposite for the degradation of sulfadiazine under solar irradiation: The indispensable effect of chloride. *Appl Catalysis B: Environ* 298:120495
22. Menazea AA, Ahmed MK (2020) Synthesis and antibacterial activity of graphene oxide decorated by silver and copper oxide nanoparticles. *J Mole Str J Mol Struct*, 128536


23. Li X, Yang X, Yi D, Liu B, Zhu J, Li J, Wang L (2021) Effects of NbC content on microstructural evolution and mechanical properties of laser clad Fe50Mn30Co10Cr10-xNbC composite coatings. *Intermetallics* 138:107309
24. Zhang T, Wang Z, Xiang H, Xu X, Zou J, Lu C (2021) Biocompatible superparamagnetic europium-doped iron oxide nanoparticle clusters as multifunctional nanoprobes for multimodal in vivo imaging. *ACS Appl Mater Interfaces* 13(29):33850–33861
25. Li Y, Macdonald DD, Yang J, Qiu J, Wang S (2020) Point defect model for the corrosion of steels in supercritical water: Part I, film growth kinetics. *Corrosion Sci* 163:108280
26. Gao M, Liu B, Zhang X, Zhang Y, Li X, & Han G (2021) Ultrathin MoS₂ Nanosheets Anchored on Carbon Nanofibers as Free-standing Flexible Anode with Stable Lithium Storage Performance. *J Alloys Compounds*, 162550
27. Li H, Wang F (2021) Core-shell chitosan microsphere with antimicrobial and vascularized functions for promoting skin wound healing. *Mater Design* 204:109683
28. Reddy CV, Koutavarapu R, Reddy KR, Shetti NP, Aminabhavi TM, Shim J (2020) Z-scheme binary 1D ZnWO₄ nanorods decorated 2D NiFe₂O₄ nanoplates as photocatalysts for high efficiency photocatalytic degradation of toxic organic pollutants from wastewater. *J Environ Manag* 268:110677
29. Koutavarapu R, Babu B, Reddy CV, Reddy IN, Reddy KR, Rao MC, Shim J (2020) ZnO nanosheets-decorated Bi₂WO₆ nanolayers as efficient photocatalysts for the removal of toxic environmental pollutants and photoelectrochemical solar water oxidation. *J Environ Manag* 265(2020):110504
30. Jung HJ, Koutavarapu R, Lee S, Kim JH, Choi HC, Choi MY (2018) Enhanced photocatalytic activity of Au-doped Au@ZnO core-shell flower-like nanocomposites. *J All Comp* 735:2058–2066
31. Koutavarapu R, Manepalli RKNR, Madhav BTP, Satyanarayana T, Nagarjuna G, Shim J, Rao MC (2020) Optical, electrical and photoluminescence studies on Al₂O₃ doped PVA capped ZnO nanoparticles for optoelectronic device application. *Optik* 205:164236
32. Li X, Yi D, Wu X, Zhang J, Yang X, Zhao Z, Liu Y (2021) Effect of construction angles on microstructure and mechanical properties of AlSi10Mg alloy fabricated by selective laser melting. *J Alloys Compounds* 881:160459
33. Lee SJ, Beglidayeva T, Jung HJ, Koutavarapu R, Yu Y, Choi M, Choi MY (2021) Plasmonic ZnO/Au/g-C₃N₄ nanocomposites as solar light active photocatalysts for degradation of organic contaminants in wastewater. *Chemosph* 263:128262
34. Jung HJ, Lee SJ, Koutavarapu R, Kim SK, Choi HC, Choi MY (2018) Enhanced catalytic dechlorination of 1, 2-dichlorobenzene using Ni/Pd bimetallic nanoparticles prepared by a pulsed laser ablation in liquid. *Cataly* 8(9):390
35. Mostafa AM, Mwafy EA, Hasanin MS (2020) One-pot synthesis of nanostructured CdS, CuS, and SnS by pulsed laser ablation in liquid environment and their antimicrobial activity. *Opt. Las. Tech.* 121:105824
36. Mostafa AM, Menazea AA (2020) Laser-assisted for preparation ZnO/CdO thin film prepared by pulsed laser deposition for catalytic degradation, *Rad Phy Chem.* 109020
37. Abdulateef S, MatJafri M, Omar A, Ahmed N, Azzez S, Ibrahim I, Al-Jumaili B, Preparation of CuO nanoparticles by laser ablation in liquid, (2016)
38. Menazea AA, Ahmed AK (2020) Synthesis and antibacterial activity of graphene oxide decorated by silver and copper oxide nanoparticles. *J Mol Struc.* 128536
39. Amiri M (2017) Antimicrobial effect of copper oxide nanoparticles on some oral bacteria and candida species. *J Den Biomater* 4(1):347–352
40. Menazea AA, Awwad NS (2020) Antibacterial activity of TiO₂ doped ZnO composite synthesized via laser ablation route for antimicrobial application. *J Mater Res Tech* 9(4):9434–9441
41. Menazea AA, Abdelbadie SA, Ahmed MK (2020) Manipulation of AgNPs coated on selenium/carbonated hydroxyapatite/ ϵ -polycaprolactone nano-fibrous via pulsed laser deposition for wound healing applications. *Appl Surf Sci* 508:145299
42. Alzoubi W, Kim MJ, Kim YG, Ko YG (2020) Dual-functional crosslinked polymer-inorganic materials for robust electrochemical performance and antibacterial activity. *Chem Eng J* 392:123654
43. Badawy S (2014) Green synthesis and characterizations of antibacterial silver-polyvinyl alcohol nanocomposite films for wound dressing. *Gre. Proc. Syntt.* 3(3)
44. Azizi S, Ahmad M, Ibrahim N, Hussein M, Namvar F (2014) Cellulose Nanocrystals/ZnO as a Bifunctional Reinforcing Nanocomposite for Poly(vinyl alcohol)/Chitosan blend films: fabrication, characterization and properties. *Int J Mole Sci* 15(6):11040–11053

45. Abdelghany AM, Menazea AA, Ismail AM (2019) Synthesis, characterization and antimicrobial activity of Chitosan/Polyvinyl Alcohol blend doped with Hibiscus Sabdariffa L. extract. *J Mole Struct* 1197:603–609
46. Abdelghany AM, Mekhail M, Abdelrazek E, Aboud M (2015) Combined DFT/FTIR structural studies of monodispersed PVP/Gold and silver nano particles. *J All Comp* 646:326–332
47. Maq B, Rahman M (2015) Improvement of Swelling Behaviour of Poly (Vinyl Pyrrolidone) and Acrylic Acid Blend Hydrogel Prepared By the Application of Gamma Radiation, *Org Chem Curr Res.* 04(02)
48. Mallakpour S, Mansourzadeh S (2018) Sonochemical synthesis of PVA/PVP blend nanocomposite containing modified CuO nanoparticles with vitamin B1 and their antibacterial activity against *Staphylococcus aureus* and *Escherichia coli*. *Ultrasonics Sonochemistry* 43:91–100
49. Rajesh K, Crasta V, Shetty G (2020) Effect of CuO nanofiller on PVA/PVP blend. *International Conference on Multifunctional Materials (ICMM-2019)*
50. Negim E, Rakhmetullayeva R, Yeligbayeva G, Urkimbaeva P, Primzharova S, Kaldybekov D (2014) Improving biodegradability of polyvinyl alcohol/starch blend films for packaging applications, *Int. J. Bas. Appl. Sci.*, 3(3)
51. Olewnik-Kruszkowska E, Gierszewska M, Jakubowska E, Tarach I, Sedlarik V, Pummerova M (2019) Antibacterial films based on PVA and PVA–Chitosan Modified with Poly(Hexamethylene Guanidine). *Poly* 11(12):2093
52. Abdullah O, Aziz S, Rasheed M (2016) Structural and optical characterization of PVA:KMnO₄ based solid polymer electrolyte. *Resul Phy* 6:1103–1108
53. Safo I, Werheid M, Dosche C, Oezaslan M (2019) The role of polyvinylpyrrolidone (PVP) as a capping and structure-directing agent in the formation of Pt nanocubes. *Nanosca Adv* 1(8):3095–3106
54. D. Kamaruddin, Edikresna, I. Sriyanti, M. Munir, M. Khairurrijal (2017) Synthesis of Polyvinylpyrrolidone (PVP)-Green tea extract composite nanostructures using electrohydrodynamic spraying technique, *IOP Conf Series: Mater Sci Eng.* 202: 012043
55. Rezeki YA, Wahyuni N, Munir MM, Khairurrijal K, Synthesis of polyvinylpyrrolidone/mango-steen pericarp extract (MPE) fibered particles using electrospray, In *Journal of Physics: Conference Series* (Vol. 1282, No. 1, p. 012033). IOP Publishing (2019, July)
56. Bryaskova R, Pencheva D, Nikolov S, Kantardjiev S (2011) Synthesis and comparative study on the antimicrobial activity of hybrid materials based on silver nanoparticles (AgNps) stabilized by polyvinylpyrrolidone (PVP). *J Chem Biol* 4(4):185–191
57. Parameswaran V, Nallamuthu N, Devendran P, Manikandan A, Nagarajan E (2018) Assimilation of NH₄Br in Polyvinyl Alcohol/Poly(N-vinyl pyrrolidone) Polymer Blend-Based Electrolyte and Its Effect on Ionic Conductivity. *J Nanosci Nanotech* 18(6):3944–3953
58. Mallakpour S, Mansourzadeh S (2018) Sonochemical synthesis of PVA/PVP blend nanocomposite containing modified CuO nanoparticles with vitamin B1 and their antibacterial activity against *Staphylococcus aureus* and *Escherichia coli*. *Ultras Sonochem* 43:91–100
59. Thi T, Tinh L, Van B, Ben P, Trung V (2012) The Effect of Polyvinylpyrrolidone on the Optical Properties of the Ni-Doped ZnSNanocrystalline Thin Films Synthesized by Chemical Method. *J of Nanomater* 2012:1–8
60. Aziz S, Hassan A, Mohammed S, Karim W, Kadir M, Tajuddin H, Chan N (2019) Structural and optical characteristics of PVA:C-Dot composites: tuning the absorption of ultra violet (UV) region. *Nanomater* 9(2):216
61. Yakuphanoglu F, Sekerci M, Ozturk O (2004) The determination of the optical constants of Cu(II) compound having 1-chloro-2,3-o-cyclohexylidinedipropyl thin film. *Opt Comm* 239(4–6):275–280
62. Aziz S, Ahmed H, Hussein A, Fathulla A, Wsw R, Hussein R (2015) Tuning the absorption of ultra-violet spectra and optical parameters of aluminum doped PVA based solid polymer composites. *J Mater Sci Mater Electr* 26(10):8022–8028
63. Aziz S (2015) Modifying Poly(Vinyl Alcohol) (PVA) from Insulator to Small-Bandgap polymer: a novel approach for organic solar cells and optoelectronic devices. *J Electr Mater* 45(1):736–745
64. Ibrahim S, Ahmad R, Johan M (2012) Conductivity and optical studies of plasticized solid polymer electrolytes doped with carbon nanotube. *J Lumin* 132(1):147–152
65. Ahmed R, Ibrahiem A, El-sayed EA (2018) Effect of Cobalt Chloride on the Optical Properties of PVA/PEG Blend, *Arab. J Nuc Sci Appl* 52(1):22–32
66. Anandalli MH, Bhajantri RF, Rathod SG, Kanakaraj TM, Chavan C, Chalawadi S (2019) Mechanical and thermal studies of brilliant green dye doped poly (vinyl alcohol) polymer composite. In *AIP Conf Proc* 2115(1):030222

67. Hammannavar PB, Baraker BM, Bhajantri RF, Ravindrachary V, Lobo B (2015) DBS investigation on films of cobalt chloride doped PVA-PVP blend. *J Phys Conf Series* 618(1):012034
68. Menazea AA, Ahmed MK (2020) Nanosecond laser ablation assisted the enhancement of antibacterial activity of copper oxide nano particles embedded though Polyethylene Oxide/Polyvinyl pyrrolidone blend matrix, *Rad Phys Chem*, 108911

Publisher's Note Springer Nature remains neutral with regard to jurisdictional claims in published maps and institutional affiliations.

Authors and Affiliations

M. F. H. Abd El-Kader¹ · Mohamed T. Elabbasy^{2,3} · A. A. Adeboye^{2,4} · A. A. Menazea^{5,6} 

¹ Biophysics Department, Faculty of Science, Cairo University, Giza, Egypt

² Department of Public Health, College of Public Health and Health Informatics, Ha'il University, Ha'il, Saudi Arabia

³ Food Control Department, Faculty of Veterinary Medicine, Zagazig University, Zagazig, Egypt

⁴ Department of Health Promotion and Behavioral Sciences, University of Texas Health Sciences at Houston, Houston, TX 77030, USA

⁵ Laser Technology Unit, Center of Excellent for Advanced Science, National Research Centre, Dokki, Giza 12622, Egypt

⁶ Spectroscopy Department, Physics Research Institute, National Research Centre, Dokki, Giza 12622, Egypt